



**HAL**  
open science

## A Survey of Complementary Methods for the Characterization of Dense Colloidal Silica

Mallorie Tourbin, Christine Frances

► **To cite this version:**

Mallorie Tourbin, Christine Frances. A Survey of Complementary Methods for the Characterization of Dense Colloidal Silica. *Particle & Particle Systems Characterization*, 2007, vol. 24 n° 6., pp.411-423. 10.1002/ppsc.200601092 . hal-00475988

**HAL Id: hal-00475988**

**<https://hal.science/hal-00475988>**

Submitted on 17 Oct 2023

**HAL** is a multi-disciplinary open access archive for the deposit and dissemination of scientific research documents, whether they are published or not. The documents may come from teaching and research institutions in France or abroad, or from public or private research centers.

L'archive ouverte pluridisciplinaire **HAL**, est destinée au dépôt et à la diffusion de documents scientifiques de niveau recherche, publiés ou non, émanant des établissements d'enseignement et de recherche français ou étrangers, des laboratoires publics ou privés.

**Published in Particle & Particle Systems Characterization, 24, 411-423 (2007)**

## **A Survey of Complementary Methods for the Characterization of Dense Colloidal Silica**

Mallorie Tourbin<sup>1</sup>, Christine Frances<sup>2</sup>

### **Abstract**

The aim of this study is to enhance existing knowledge for using different techniques developed for characterization of stability and particle sizing of nanoparticles in dense dispersions subjected to interparticular and hydrodynamic forces. Silica suspension, commercially known as Klebosol® 30R50 and containing particle size 80 nm on average, was investigated in the study over a wide range of concentrations. The investigations were carried out using different optical and acoustic techniques such as laser diffraction, multiple light scattering, photon correlation spectroscopy and acoustic spectroscopy. The study brings out capabilities and limitations of these modern techniques based on different physical principles behind the characterization of size distribution of particles in suspensions. The results are presented in terms of particle size range, solid concentration and technological aspects such as on-line and off-line analysis. An important finding is that at higher concentrations many of these modern techniques need to be improved because the standard models become practically invalid because of complex interaction of acoustic and optical waves with particles in suspensions of silica.

*Keywords:* acoustic spectroscopy, dense suspensions, granulometry, nanoparticles, stability.

---

<sup>1</sup> Mallorie Tourbin, Dr.

<sup>2</sup> Christine Frances, Dr. HDR

Laboratoire de Génie Chimique CNRS/INPT/UPS UMR 5503,

5, rue Paulin Talabot, BP 1301, 31106 Toulouse Cedex 01, France

Corresponding author : Christine Frances tel : 33 (0)5 34 61 52 24 [Christine.Frances@ensiacet.fr](mailto:Christine.Frances@ensiacet.fr)

## **1. Introduction**

The significance of nanoparticles is increasing with increasing industrial interest. It is important to enhance existing knowledge for characterization of colloidal dispersions because this knowledge provides direct basis for process control, process optimization and improving quality of product e.g. improvement in optical properties, texture, rheological properties, bioavailability etc. Indeed, particle size distribution and stability of the suspension are two key factors for the successful production of a large number of industrial products [1].

There are many methods that are used for the characterization of stability of colloidal dispersions. e.g. sedimentation [2, 3], turbidity [4, 5] and zeta potential [6].

For particle sizing, there exist many techniques as well, with their own advantages and limitations. Optical methods, photon correlation spectroscopy and multiple light scattering methods are name of few conventional techniques. The conventional optical methods generally require dilution of the suspension which can involve a change of the dispersion state of the system, modifying the physico-chemical properties of the suspension, thus inducing an aggregation or de-agglomeration process of the dispersed phase. Even the photon correlation spectroscopy method has been found to be inadequate for direct particle sizing on highly concentrated slurries. Multiple light scattering methods are often used since sometimes they may bring interesting information on microstructural changes of concentrated suspensions [7]. Apart from the conventional techniques, some sophisticated techniques such as SEM [8], rheology analysis [3, 9], acoustic spectroscopy [10-12], etc., have been reported in recent past for the characterization of concentrated slurries.

The existence of many methods and techniques causes problems in choosing the right one for characterization of colloidal dispersions because each technique is not valid for all type of materials, for all the particle sizes, for all the process conditions, and for all the concentration ranges etc. The aim of this study is to enhance existing knowledge for using different

techniques developed for characterization of stability and particle sizing of nanoparticles in dense dispersions by pointing the capabilities and limitations of various techniques and technologies. The study focuses on characterization of dense colloidal silica suspensions using several complementary optical and acoustic methods such as laser diffraction, multiple light diffusion, photon correlation spectroscopy and acoustic spectroscopy. The stability of the silica suspensions was previously established over a large concentration range measuring pH, zeta potential and turbidity.

## **2. Physical Principles of Optical and Acoustic Methods used for Particle Sizing and Stability Analysis**

Particle size and stability are variables of significant interest to many manufacturers, as they have a direct impact on the quality of the finished product. Optical properties, such as opacity, tinting strength, undertone, film appearance, as well as bulk properties, including dispersion and flocculation characteristics, and viscosity, are all, to some extent, a function of particle size and dispersity. The size distribution of nanoparticles suspended in liquids is a critical parameter in a multitude of industries and applications. The following sections describe physical principles behind optical and acoustic methods used for particle sizing and stability analysis.

### **2.1 Multiple Light Scattering**

Multiple light scattering techniques consider the interaction of a focused light beam with particles randomly distributed in a fluid. Incident photons undergo multiple scattering events before absorption, backscattering or transmission through the sample. In the framework of the photon diffusion approximation, the characteristic lengths involved in conservative light scattering (i.e. without absorption phenomena) are the photon mean path,  $\lambda$  (average distance

between two scattering events in the medium) and the transport mean path,  $\lambda^*$  (decorrelation length between the direction of the photon propagation and the incident direction). For a random distribution of scatterers, mean path lengths  $\lambda$  and  $\lambda^*$  are dependant upon the physical properties of the scattering medium (refractive index  $n_f$  of suspending fluid, refractive index  $n_p$  of particles, average particle diameter  $d$  and particle volume fraction  $\phi$  [13] :

$$\lambda = \frac{2d}{3\phi Q} \quad (1)$$

$$\lambda^* = \frac{\lambda}{1-g} = \frac{2d}{3\phi(1-g)Q} \quad (2)$$

where  $Q$  is the scattering efficiency (ratio of total scattering cross-section and geometrical cross-section  $\pi d^2/4$  of a particle). The asymmetry parameter  $g$  represents the average cosine of scattering angles from a single particle and describes the anisotropy of the scattering diagram ( $g=0$  for isotropic Rayleigh scatterers and  $0.5 < g < 1$  for Mie scatterers of sizes larger than the light wavelength).  $Q$  and  $g$  optical parameters depending both upon  $n_p/n_f$  and  $d$  can be determined from the Mie theory. Dependent scattering effects arising from spatial particle correlations may further influence the scattering efficiency factor in concentrated suspensions for particles smaller than the wavelength. For nonabsorbing Rayleigh scatterers, the Perkus Yevick approximation for the pair distribution gives an analytical expression of the photon mean path taking into account the particle correlations:

$$\lambda = \frac{2d}{3\phi(1-g)Q} \frac{(1+2\phi)^2}{(1-\phi)^4} \quad (3)$$

## 2.2 Dynamic Light Scattering Technique: Photon Correlation Spectroscopy

The Photon Correlation Spectroscopy (PCS) allows measuring size below the limit of the static light scattering and diffraction methods which is almost 50 nm. For this study, a Zetasizer Nano S (Malvern Instruments) was used. The principle of this instrument is based

on the Brownian motion of the particles. The frequency and the amplitude of this motion depend on the size of the particle and the viscosity of the solvent. PCS has proved to be a valuable tool for the determination of particle sizes in the submicron range. Since PCS is a technique that probes the dynamics of dispersed particles detecting the backscattered light (angle of  $173^\circ$ ) of the suspensions, more information than particle size distribution can be obtained. In particular, for particles subjected to Brownian motion, the translational diffusion coefficient (the collective one, which describes the motion of a collection of particles) can be determined by PCS [14-15].

For dilute suspensions, where the effect of interactions can be neglected, the diffusion coefficient  $D_0$  is related to the particle diameter  $d$  by the well known Stokes-Einstein law:

$$D_0 = \frac{k_B T}{3\pi\eta d} \quad (4)$$

Since the colloidal silica suspensions are stabilized by particle interactions, their effect cannot be neglected. Particle interactions result in a dependence between the concentration and the diffusion coefficient and, instead of neglecting this relationship, it can be exploited to put in evidence particle interaction. It will be assumed that dispersed particles are rigid monodisperse spheres. According to Einstein [16], the process of diffusion is driven by an osmotic pressure gradient and counteracted by a friction force. The balance of these forces results in the following expression for the diffusion coefficient:

$$D = b \left( \frac{\partial \Pi}{\partial n} \right)_{T,P} \quad (5)$$

Where  $b$  is the mobility of the dispersed particles,  $\Pi$  represents their osmotic pressure and  $n$  is the particle number density (number of particles per unit volume). Since both  $\Pi$  and  $b$  are affected by particle interactions, the diffusion coefficient  $D$  is also dependent on it. At finite concentration, the effect of particle interactions can be taken into account by expanding  $\Pi$  and

$b$  in a power series of concentration. The final concentration dependence of the diffusion coefficient can be written as [17-18] :

$$D = D_0(1 + k_D\phi + \dots) \quad (6)$$

where

$$k_D = \lambda + \frac{2B_2}{v} \quad (7)$$

and  $v$  represents the volume of a single spherical particle,  $\lambda$  and the coefficient  $B_2$  can be related to the potential of the mean force between two particles.

### 2.3 Acoustic Spectroscopy

Sound waves interact in a similar manner to light waves but have the advantage that they can travel through concentrated suspensions and emulsions. The interaction of ultrasound waves with particles has been comprehensively described through a complete mathematical framework which accurately predicts the attenuation spectrum of any suspension. A rigorous but complex model, known as the ECAH model, has been published by Epstein and Carhart (1953) [19] and Allegra and Hawley (1972) [20] which predicts the scattering of an acoustic plane wave by a sphere of a given size. When a sound wave passes through a suspension, changes occur to the wave as well as to the two phases of the particulate medium. A particle presents a discontinuity to sound propagation and the wave scatters with a redistribution of the acoustic energy throughout the volume before being detected at the receiver (scattering and diffraction losses). In addition, absorption phenomena occur when particles move relative to the suspending medium and the mechanical energy degrades by shear friction (viscous losses). Furthermore, temperature differences develop between phases because of the thermodynamic coupling between the pressure and thermal waves that move in phase (thermal losses). In the ECAH theory, any of these attenuation phenomena are accurately characterized through fundamental equations based on the laws of conservation of mass,

energy, and momentum, the thermodynamic equations of state, and stress-strain relations for isotropic elastic solids or viscous, by formulating the Wave Equations which describe the interaction between the sound wave and the particles.

### **3. Colloidal Silica Suspensions**

A colloidal silica suspension, Klebosol 30R50 (Clariant, France), having an initial solid content of 30% wt. was used. Its density is about  $1.21 \text{ g.cm}^{-3}$  (silica density is  $2.37 \text{ g.cm}^{-3}$ ) and its specific surface is around  $50 \text{ m}^2.\text{g}^{-1}$ .

It was observed by scanning electronic microscopy that silica particles of Klebosol 30R50 were spherical and monodispersed. Their average number diameter was roughly estimated at 80 nm.

Deionized water (pH~6 and  $\Lambda \sim 5\text{-}7 \text{ }\mu\text{S}$ ) was used to prepare diluted silica suspensions from the Klebosol 30R50 initial suspension. The solid content of these suspensions is determined with a precision of  $10^{-2} \%$ , by the measure of the humidity rate by thermogravimetry using a Halogen Moisture Analyser HB43 desiccation balance (Mettler Toledo). For this purpose, a few grams of sample is heated by an infrared radiation of a halogenous source and the sample mass is continuously measured during the drying process. The mass concentration is then converted into volume concentration taking into account the silica density ( $2.37 \text{ g.cm}^{-3}$ ) and the density of the suspension (between  $1.21$  and  $1 \text{ g.cm}^{-3}$  depending on the concentration).

### **4. Stability and Physico-Chemical Properties of Silica Suspensions**

Colloidal dispersions are inherently thermodynamically unstable systems which can be considered as kinetically stable if the destabilization rate is small enough compared with the expected lifespan. The analysis of the dispersion instability is of prime importance.

The two major destabilization phenomena, affecting the homogeneity of dispersions are particle migration, which is due to differences of density between the dispersed and the

continuous phases (creaming and sedimentation phenomena) and particle size variation, which is due to the modifications of size of the particles (flocculation, coagulation or aggregation).

The physico-chemical properties of the silica suspensions: pH, zeta potential and turbidity were analyzed in order to estimate the stability of the suspensions.

#### **4.1 pH, Zeta potential and Interaction Energy Diagram**

The pH of the medium has a strong influence on the stability of colloidal silica suspensions. Indeed, the gelation rate is very high for pH values close to 4 or 5. However, below this critical zone of pH, and around the isoelectric point (pH  $\sim$  2), the suspension is stabilized by hydrogen bonds that are formed between the silica particles and the continuous phase. Above this pH, and more particularly for pH > 8, the suspension is stabilized by electrostatic repulsions [21].

pH measurements were done with a standard MeterLab Radiometer analytical PHM210 pH-meter and a combined pH electrode PHC3001-8 which is especially designed for aqueous suspensions. The initial silica suspension has a solid content of 15.32 % v/v and a pH of 8.95. Diluting the suspension until 0.43 % v/v, the pH of the suspension does not fluctuate a lot and remains between 7.73 and 9.25 with a precision of 0.02 on pH. So, over that range of concentration, the pH value ensures stabilization by electrostatic repulsions.

The magnitude of the zeta potential gives an indication of the potential stability of the colloidal system. For the suspension studied, the zeta potential was found to be -56.1 mV at pH = 8.42. The stability is strengthened by sodium ions that adsorb on the silanol groups (Si-OH), which increase the charge of the particle surfaces and increase the range of the electrostatic repulsion forces (see Figure 1) [21].

Moreover, the relative importance of physico-chemical interactions and Brownian dispersion forces can be estimated using the following ratios:

$$\frac{\text{attractive forces}}{\text{diffusion}} = \frac{A_{eff}}{kT} = 2.01 \quad (8)$$

$$\text{and } \frac{\text{electrostatic forces}}{\text{diffusion}} = \frac{\varepsilon\varepsilon_0\psi_s^2 r}{kT} = 21.1 > 1 \quad (9)$$

with  $A_{eff} = 0,83.10^{-20} J$  Hamaker's constant for silica in water,  $k$  Boltzmann's constant,  $T$  the temperature, chosen at 25 °C,  $\varepsilon = 80$  the dielectric constant of water,  $\varepsilon_0 = 8,854.10^{-12} C^2 J^{-1} m^{-1}$  the vacuum permittivity,  $\psi_s$  silica surface potential, taken in a first approximation as equal to the zeta potential ( $\psi_s \approx \zeta = -56,1 mV$  at  $pH=8,42$ ) and  $r = 40.10^{-9} m$  the silica particle radius. The values of the ratios approximated by equations (8) and (9) confirm the fact that the suspension is stabilized by electrostatic repulsions.

The stabilization of the suspension by electrostatic repulsions can also be interpreted on the interaction energy diagram knowing the salt concentration of the suspension (characterized by ICP Spectroscopy):  $[Na^+] = 7.8 10^{-5} mol.L^{-1}$ . Then the attractive and repulsive interaction energies can be calculated in diluted conditions by the DLVO theory. For particles of 80 nm of Klebosol 30R50, the diagram of potential energy is drawn on Figure 1. It is confirmed again that the attractive interactions are negligible in comparison with the repulsive interactions that ensures the stability of the system.

Figure 1

## 4.2 Silica Suspension Stability Analysis

The stability of silica suspensions was measured with a Turbiscan MA 2000 (Formulacion, France) based on multiple light scattering principle.

The dispersion is put into a flat-bottomed glass cylindrical cell. A LED that emits in the near infrared ( $\lambda=850$  nm) gives light to the glass tube and two photo-detectors collect the transmitted and backscattered light by the dispersion. The detection head scans the entire height of the sample (about 65 mm), acquiring transmission and backscattering data. The apparatus allows detecting the phenomenon of particles migration (creaming, sedimentation) and particle size variations [22]. It is important to note that this technique does not give direct spatial information, but information on the motion of the particles.

As described before, the photon transport length for dependent diffusion can be determined from the Percus-Yevick model. The modelling was made for silica particles of various refractive index (1.44 - 1.45) and size (between 70 and 100 nm). The best fit between experimental measurements and the theoretical Percus-Yevick curve was found for a refractive index of 1.44 and a particle diameter of 80 nm (Figure 2). The use of the model highlights that in the concentrated regime ( $\phi>10\%$ ), the diffuse transmittance increases with particle volume fraction as a result of dependent scattering whereas in the diluted regime (independent scattering regime) ( $\phi<10\%$ ), the diffuse transmittance decreases with particle volume fraction.

Figure 2

Particle migration and particle size variation analyses were made measuring the transmission fluxes versus the height of the cell each 40 min during approximately 5 days and a half. Figures 3a and 3b present transmission level for two suspensions, at 15.3% and 1.3% v/v versus time at three different points of the measurement cell: the top, the middle and the bottom of the cell.

For the more concentrated suspension (15.3% v/v), the transmitted flux increases versus time along the entire measurement cell. In case of dependent scattering (interferences between the scattered waves), an increase of the transmitted flux would be interpreted by two ways. On one side, if the particle concentration of the sample remains constant, an increase of the transmitted flux could only be due to a decrease of the particles size (de-agglomeration or fragmentation). On the other side, if the size of the particles remains constant, an increase of the transmitted flux could only be due to an increase of the particle concentration. These two scenarios are impossible in our case and probably, this evolution indicates a structuring of the suspension modifying its optical properties thus inducing an increase of the transmitted flux. For the diluted suspension (1.3% vol.), a migration of particles is observed. Indeed, the clarification of the suspension is indicated by the increase of the diffuse transmittance at the top of the cell and the sedimentation of the particle is indicated by the decrease of the diffuse transmittance at the bottom of the cell. However, these phenomena are not very significant and such analysis demonstrates a relative good stability of the silica suspension.

Figure 3a and Figure 3b

## **5. Particle Size Characterization: Experimental Results**

### **5.1 Characterization of PSD in Diluted Conditions by Laser Diffraction**

The size distribution of particles suspended in diluted conditions was first characterized by the well-known laser diffraction method. By this technique, in the submicronic range, the PSD are determined on the base of the Mie theory. The results in term of number and volume particle size distributions are shown on Figure 4. It is obvious that the distributions are deeply dissimilar according to the parameter taken into account: number or volume; the values taken by the parameters of the curves (mean diameter, height of the mode, etc.) are also different.

The conversion of one distribution to the other is possible making some hypothesis on the shape and the density of the particles. As a result, the mean size is about  $84 \text{ nm}$  considering a number distribution which is coherent with SEM observations, and about  $112 \text{ nm}$  for a volume distribution.

Figure 4

## 5.2 Characterization of PSD in Dense Conditions by Multiple Light Scattering

For a first approximation, measurements of a mean particle size (Sauter diameter,  $d_{32}$ ) in concentrated conditions and under flow were made by multiple light scattering using a Turbiscan On-Line apparatus (Formulation). The measurements were made for 1 liter of different suspensions of Klebosol 30R50 from 15.3% to 1.3% v/v placed in a tank and put in circulation with a peristaltic pump. The optical analyser, comprising the emitting near-infrared focused LED (wavelength = 850 nm) and the transmission ( $135^\circ$  with respect to the incident light) and backscattered light ( $45^\circ$ ) detectors was placed on the derivative loop allowing on-line analysis. The diffuse transmittance level is defined as the ratio between the light flux  $f_T$  and the light flux  $f_{T0}$  transmitted through a non absorbing standard fluid:

$$T_r = \frac{f_T}{f_{T0}} = e^{-\frac{2r_i}{\lambda(\phi,d)}} = e^{-\frac{3r_i\phi Q}{d}} \quad (10)$$

with  $r_i$  the intern radius of the cell,  $\lambda$  the photon mean path,  $\Phi$  the particle volume fraction,  $d$  the particle diameter and  $Q$  the scattering efficiency.

The analysis was realized during 300s and each measurement was performed after an interval of 3s. The values of the mean diffuse transmittance measured are reported in Table 1. They show that the diffuse transmittance decreases when the concentration increases. As it was shown previously, the dependent scattering regime occurring for almost all the considered

concentration ranges and spatial particle correlations must be taken into account. The Percus-Yevick model was then used to model the evolution of the diffuse transmittance versus particle diameter for different concentrations (Figure 5). It can be observed that for a given concentration, the diffuse transmittance decreases when the particle diameter increases and then, for each concentration, the mean diameter in case of particle structuring corresponding to the measured diffuse transmittance may be calculated. The values of particle diameter are reported in Table 1. They are quite homogeneous over the concentration range and approximately equal to 90 nm. However, due to the presence of a transmittance shaft versus concentration (cf. Figure 2), it is obvious that such a technique cannot give a precise value of silica particle size in dense conditions.

Table 1

Figure 5

### **5.3 Characterization of PSD in Dense Conditions by Photon Correlation Spectroscopy**

The size distributions of silica suspensions at different concentrations were characterized by Photon Correlation Spectroscopy using the Zetasizer Nano S (Malvern Instruments). For very diluted suspension (volume concentration < 0.43%), the mean size or the Z-average size determined by the software of the apparatus is almost constant for the different concentrations i.e. *85.3 nm* on average (Figure 6) (reproducibility ~1%). This graph puts in evidence a range of concentration in which the size is independent of silica concentration. Within this range, the particle interactions can be neglected and the mean size is calculated applying directly the Stokes-Einstein law. The Z-average size is a hydrodynamic diameter corresponding to the diameter of a sphere that has the same translational diffusion coefficient as the particle. Figure 7 shows the full particle size distributions calculated by the software with the partial list

square method for the concentrations lower than 0.43% v/v. The calculated size distributions are quite similar.

Figure 6

Figure 7

When the volume concentration is higher than 0.43%, the *Z*-average size linearly decreases versus the concentration. Xu (2000) explains this trend by a modification of the structural factor due to the interaction between particles [23].

In order to highlight the interaction effects, results are also reported on the Figure 6 corresponding to measurements done modifying the solution salinity by the addition of a KCl solution at  $10^{-2}$  M. The graph clearly proves that the *Z*-average size depends on the particle interactions. Indeed, the average size, *Z*, defined as the Stokes-Einstein diameter, decreases with an increasing concentration for repulsive interactions. An opposite evolution would be observed if attractive interactions were dominant. If the diffusion coefficient is defined as:

$$D = \frac{k_B T}{3\pi\eta z} \quad (11)$$

It is then possible to extract it from the values of the average size. The dependence of the diffusion coefficient *D* versus concentration for the studied silica suspensions can be represented by equation (6). The values of the translational diffusion coefficient  $D_0$  are then evaluated (see Table 2). From  $D_0$ , the hydrodynamic diameter  $d_H$ , which is the diameter of the particle plus the thickness of the layer of solvation which surrounds it, is obtained [15]:

$$D_0 = \frac{k_B T}{3\pi\eta d_H} \quad (12)$$

The silica particle diameter can then be calculated knowing the value of the Debye length, as shown by equation (12):

$$d_H = d + \frac{1}{\kappa} \quad (13)$$

Where [24]:

$$\frac{1}{\kappa} = \frac{0.304}{\sqrt{[monovalent\ salt]}} \quad (14)$$

The concentration of monovalent salt is  $[monovalent\ salt]=[Na^+]=7.8 \cdot 10^{-2} \text{ mol.L}^{-1}$  for the initial suspension, and  $[monovalent\ salt]=[Na^+]+[KCl]=1.078 \cdot 10^{-2} \text{ mol.L}^{-1}$  for the second suspension.

Table 2 shows that a little addition of salt involves a compression of the double layer; it is the reason why the hydrodynamic diameter decreases when the salinity increases. From these results, it is concluded that more precise values of the particle size would be obtained by PCS in dense conditions modifying the solution salinity in order to reduce the double layer thickness.

Table 2

#### 5.4 Acoustic Spectroscopy

Finally, acoustic spectroscopy was used to characterize the particle size distribution of silica suspensions on the whole range of concentration. In this work, we had access to the commercial acoustic spectrometer Ultrasizer (Malvern Instruments). The Ultrasizer measures the acoustic attenuation spectrum of the sample over the frequency range of 1-150 MHz. The physical properties that would be used by the software for the system silica-water are reported on Table 3. The Ultrasizer measures the attenuation of the ultrasonic wave through the suspension for different frequencies. However instead of the total attenuation, it sounds more relevant to consider the excess of attenuation only due to the particles in the medium and not to the intrinsic attenuation of each phase. The excess of attenuation,  $\alpha_e$ , is then:

$$\alpha_e = \alpha_t - \phi\alpha_{pd} - (1 - \phi)\alpha_{pc} \quad (15)$$

were  $\alpha_t$  is the total attenuation,  $\alpha_{pd}$  the attenuation of the dispersed phase,  $\alpha_{pc}$  the attenuation of the continuous phase and  $\phi$  the volume concentration of the dispersed phase.

The attenuation spectrum of water was measured and fitted by a second order equation as a function of the frequency. Assuming that the attenuation of the solid phase is negligible compared with the attenuation of the liquid phase, the equation of the excess of attenuation can finally be expressed by:

$$\alpha_e(f) = \alpha_t - (1 - \phi)(0,0047f^2 - 0,0083f) \quad (16)$$

Figure 8 reports the excess of attenuation versus the frequency for different concentrations of Klebosol 30R50. The attenuation spectra are parallel (reproducibility~1.5%). Despite of the relative high density of silica, the dominant attenuation effect, indicated by the trend of the curves, is due to thermo-elastic interactions because of the small size of particles.

Table 3

Figure 8

Theoretically, the attenuation is proportional to the concentration of the suspended particles and moreover, when the thermo-elastic effects are predominant, the attenuation is also a function of the wave frequency [20]. Thus, normalizing the spectra by the frequency and the concentration, the curves should be superimposed. But the normalized spectra (Figure 9) do not coincide (the distance between two curves goes from 3 to 20 %). The trend of these curves highlights the existence of particle interactions which modifies the behaviour of the wave, also described as a multiple scattering phenomenon. Multiple scattering is increased at higher concentrations and it is the reason why the curves are almost linear for the higher concentrations while for the more diluted suspensions, they are more curved.

Figure 9

Figure 10 confirms the existence of multiple scattering because in the absence of the particle-particle interaction, contribution of the particles to the total attenuation is additive. As a result, it is a linear function of the volume fraction. But particle interaction affects the dissipation of the acoustic energy caused by each particle and their contribution to the total attenuation is not proportional to their volume any more but depends on the presence of other particles and interparticle distance. As shown by Hipp et al. [25], Figure 10 puts in evidence that the ECAH theory does not give a good prediction of the evolution of attenuation with the concentration and the frequency in case of multiple scattering. Indeed, experimental data highlights that attenuation excess versus frequency decreases for high frequencies in comparison with the behaviour of an isolated particle (predicted by the ECAH theory). Moreover, the theory does not predict a so high dependence of the attenuation versus frequency. The deviation in comparison with the behaviour of an isolated particle is more pronounced for low frequencies. The interaction between particles may be quantified by the calculation of boundary layers or ‘skin depths’. Thermal waves decrease rapidly in a thin boundary layer around the particle. The thickness of the layers associated to viscous,  $\delta_v$ , and thermal,  $\delta_t$ , waves can be estimated by the following expressions based on the physical properties of the continuous phase [26].

$$\delta_v = \sqrt{\frac{2\eta}{\omega\rho}} \quad (17)$$

and

$$\delta_t = \sqrt{\frac{2k_T}{\omega\rho C_p}} \quad (18)$$

with  $\eta$  the fluid viscosity,  $\omega=2\pi f$  the angular frequency,  $\rho$  the fluid density,  $k_T$  the thermal conductivity of the fluid and  $C_p$  the heat capacity of the fluid.

It is apparent from Figure 11, that overlapping starts, for example, at about 7% v/v and 10 MHz, and becomes more pronounced the higher the particle concentration (decreasing  $s$ ) or

the lower the frequency (increasing  $\delta$ ). This behaviour is in agreement with that observed experimentally. The overlapping is important for the whole concentration range, especially for low frequencies, and it is even total for concentrations higher than 4.5% v/v.

Figure 10

Figure 11

From the attenuation spectra, the determination of the particle size distribution can be done by the Ultrasizer software on different ways. Imposing a monomodal size curve, the distributions were first calculated introducing the real particle concentration. The corresponding curves are drawn on Figure 12. Those distributions, and particularly the one at 15.30% v/v, are very different from each other. Furthermore, the mean diameters are very far from those expected ones. In second step, the size distributions were calculated imposing the mean diameter (equal to the volume mean size obtained by laser diffraction = 112nm). The distributions, drawn on Figure 13, are very similar whatever the solid concentration, but the residuals values which characterize the fitting between the experimental and calculated attenuation spectra were not good. The calculated solid concentrations were also very different to the real ones. However, the discrepancy between the real and the calculated concentrations decreases with the concentration. Finally, the Ultrasizer software was used to calculate the theoretical attenuation spectra corresponding to a log-normal particle size distribution defined by its two characteristic parameters: a geometric mean size = 112 nm and a geometric standard deviation = 1.5 (those parameters correspond to the fitting by a log-normal law of the size distribution of a diluted suspension of silica measured by laser diffraction). Comparing those spectra to the experimental ones (see Figure 14), it can be seen that the theoretical spectra are parallel to one another but they are not parallel to the experimental spectra. From these results, it is clear

that the introduction of a simple correction factor is not enough to compensate the deviation on attenuation spectra due to multiple diffraction and thus to obtain a correct particle size distribution in dense conditions.

Figure 12

Figure 13

Figure 14

## **6. Conclusion**

Different methods were used to characterize the stability and the size distribution of silica nanoparticles in suspension over a large range of concentration, until 15 % v/v. The stability of suspensions was measured analyzing the transmitted flux by the suspension versus time. No important particle migration or physico-chemical destabilization phenomena were detected. Concerning the particle size characterization, not any system was able to give a correct particle size distribution over the full range of concentration considered, but important information was obtained on this dispersed medium by the use of different complementary methods:

- A mean diameter may be estimated from on-line analysis based on multiple light scattering by means of the Percus-Yevick model taking into account the particle interactions for dependant diffusion in dense conditions. It is then possible to have an estimation of the mean diameter of Klebosol silica particles for the entire concentration range studied here.
- The Photon correlation spectroscopy allows measuring the size distribution of particles in terms of hydrodynamic diameter from which the particle diameter can be derived, calculating the Debye length. By this technique, the good particle size

distributions were obtained for the diluted suspensions ( $\Phi < 0.43\%$ ). But for higher concentrations, calculations are needed to determine the real particle diameter.

- Using acoustic spectroscopy, the dominant mechanism of sound attenuation for silica nanoparticles in dense suspensions was identified to be thermo-elastic in nature due to the very small particles size. Calculating the viscous and thermal skin depths, the multiple scattering phenomenon was quantified and it was concluded that the ECAH theory can not be extended in that case in order to derive a correct particle size distribution. However, the sound attenuation spectrum is a crude and pure response containing important information on the physical properties of particles in suspension and future papers will discuss how it is possible to exploit acoustic spectroscopy to get information on particle size and structure on-line of an aggregation process. On the contrary of the previous techniques, by this method, good analyses are possible only for Klebosol silica suspensions relatively concentrated ( $\Phi > 0.43\%$ ).

## 7. Acknowledgements

The authors gratefully acknowledge R. Tweedie and M. Terray from Malvern Instruments for their scientific support on acoustic spectroscopy analysis. The authors are also very grateful for the local support of the cooperative structure of joint research FERMaT (Toulouse, France).

## 8. Nomenclature

$A_{eff}$	Hamaker's constant (J)
$b$	Particles mobility ( $s.kg^{-1}$ )
$C_p$	Heat capacity ( $J.K^{-1}$ )
$d$	Particle diameter (m)

$d_H$	Hydrodynamic diameter (m)
$d_{32}$	Sauter Diameter (m)
$D$	Diffusion coefficient ( $\text{m}^2 \cdot \text{s}^{-1}$ )
$D_0$	Translational diffusion coefficient ( $\text{m}^2 \cdot \text{s}^{-1}$ )
$F$	Frequency (Hz)
$g$	Asymmetry parameter (-)
$k_B$	Boltzmann constant ( $k_B = 1.381 \cdot 10^{-23} \text{ J} \cdot \text{K}^{-1}$ )
$k_T$	Thermal conductivity ( $\text{W} \cdot \text{m}^{-1} \cdot \text{K}^{-1}$ )
$n$	Particle number density ( $\text{m}^{-3}$ )
$n_p$	Particles refractive index (-)
$Q$	Scattering efficiency (-)
$r$	Particle radius (m)
$r_i$	intern radius of the Turbiscan cell (m)
$T$	Temperature (K)
$v$	Volume of the particle ( $\text{m}^3$ )
$v/v$	Volume fraction of particles (-)
$wt.$	Mass solid fraction (-)
$z$	Z-average size measured by PCS (m)

#### *Greek Letters*

$\alpha$	Sound attenuation ( $\text{dB} \cdot \text{inch}^{-1}$ or $\text{Np} \cdot \text{m}^{-1}$ )
$\delta_v$	Thickness of the viscous layer (m)
$\delta_t$	Thickness of the thermal layer (m)
$\varepsilon$	Relative dielectric constant of water (-)
$\varepsilon_0$	Vacuum permittivity ( $\varepsilon_0 = 8.854 \cdot 10^{-12} \text{ C}^2 \cdot \text{J}^{-1} \cdot \text{m}^{-1}$ )
$\Phi$	Particle volume fraction (-)

$\eta$	Viscosity (Po)
$\kappa$	Debye length ( $\text{m}^{-1}$ )
$\lambda$	Photon mean path (m)
$\lambda^*$	Transport mean path (m)
$A$	Conductivity (S)
$\Pi$	Osmotic Pressure (Pa)
$\rho$	Density ( $\text{kg.m}^{-3}$ )
$\psi$	Surface potential (V)
$\omega$	Angular frequency ( $\text{rad.s}^{-1}$ )
$\zeta$	Zeta potential (V)

*Acronym:*

DLVO	Theory of Derjaguin, Landau, Verwey and Overbeek
ECAH	Theory of Epstein, Carhart, Allegra and Hawley
PCS	Photon Correlation Spectroscopy

## 9. References

- [1] B. Singh, R. Menchavez, M. Fuji, M. Takahashi, Characterization of concentrated colloidal ceramics suspension: A new approach, *J. Colloid Interface Sci.* **2006**, in press.
- [2] W. J. Tseng, C. H. Wu, Sedimentation, rheology and particle-packing structure of aqueous Al<sub>2</sub>O<sub>3</sub> suspensions, *Ceramics International* **2003**, 29 (7), 821-828.
- [3] B. J. Briscoe, A. U. Khan, P. F. Luckham, Stabilising zirconia aqueous suspensions using commercial polyvalent electrolyte solutions, *J. of the Eur. Cer. Soc.* **1998**, 18 (14), 2169-2173.
- [4] J. L. Trompette, M. Meireles, Ion-specific effect on the gelation kinetics of concentrated colloidal silica suspensions, *J. Colloid Interface Sci.* **2003**, 263 (2), 522-527.

- [5] F. Gruy, M. Cournil, Silica aggregate sizing, PARTEC **2004**, Nuremberg, Germany.
- [6] S. Sadasivan, D. H. Rasmussen, F. P. Chen, R. K. Kannabiran, Preparation and characterization of ultrafine silica, *Colloids and Surfaces A: Physicochemical and Engineering Aspects* **1998**, 132, 45-52.
- [7] C. Bordes , P. Snabre, C. Frances, B. Biscans, Optical investigation of shear-and time-dependent microstructural changes to stabilized and depletion-flocculated concentrated latex sphere suspensions, *Powder Technol.* **2003**, 130, 331-337.
- [8] S. H Im, T. Herricks, Y. Tack Lee, Y. Xia, Synthesis and characterization of monodisperse silica colloids loaded with superparamagnetic iron oxide nanoparticles, *Chem. Phys. Letters* **2005**, 401(1-3), 19-23.
- [9] J. A. Yanez, E. Laarz , L. Bergström, Viscoelastic Properties of Particle Gels, *J. Colloid Interface Sci.* **1999**, 209, 162-172.
- [10] F. Alba , G. M. Crawley, J. Fatkin , D. M. J. Higgs, P.G. Kippax, Acoustic spectroscopy as a technique for particle sizing of high concentration colloids, emulsions and suspensions, *Colloids and Interfaces A: Physicochemical and Engineering Aspects* **1999**, 153, 495-502.
- [11] A. K. Hipp A.K., G Storti , M. Morbidelli, Acoustic Characterization of Concentrated Suspensions and Emulsions 2. Experimental Validation, *Langmuir* **2002**, 18, 405-412.
- [12] A. S. Dukhin , P. J. Goetz, Characterization of chemical polishing materials (monomodal and bimodal) by means of acoustic spectroscopy, *Colloids and Surfaces A: Physicochemical and Engineering Aspects* **1999**, 158, 343-354.
- [13] P. Snabre, A. Arhaliass, Anisotropic scattering of light in random media. Incoherent backscattered spot light, *Applied Optics* **1998**, 37 (18), 211-225.
- [14] G. K. Batchelor, Brownian diffusion of particles with hydrodynamic interaction, *J. Fluid Mechanics* **1976**, 74 (1), 1-29.
- [15] R. Finsy, Use of One-Parameter Models for the Assessment of Particle Interactions by

Photon Correlation Spectroscopy, *Part. Part. Syst. Charact.* **1990**, 7, 74-79.

[16] A. Einstein, Elementare Theorie der Brownschen Bewegung, *Z. Electrochem* **1908**, 14, 235-239.

[17] M. Stimson, G. Jeffery, *Proc. R. Soc. London, Ser. A* **1926**, 111, 110-127.

[18] R. Goldman, R. Cox, H. Brenner, The slow motion of two identical arbitrarily orientated spheres through the viscous fluid, *Chem. Eng. Sci.* **1966**, 21, 1151-1170.

[19] P. S. Epstein, R. R. Carhart, The absorption of sound in suspensions and emulsions. I. Water fog in air, *Journal of Acoustic Society of America* **1953**, 25, 553-565

[20] J. R. Allegra, S. A. Hawley, Attenuation of Sound in Suspensions and Emulsions: Theory and Experiments, *Journal of Acoustic Society of America* **1972**, 51 (5 part 2), 1545 - 1564.

[21] R. K. Iler, *The Chemistry of silica*. Wiley, New York, **1979**.

[22] O. Mengual, G. Meunier, I. Cayré, K. Puech, P. Snabre, TURBISCAN MA 2000: multiple light scattering measurements for concentrated emulsion and suspension instability analysis, Atlanta, **1999**, 445-456.

[23] R. Xu, Particle characterisation: light scattering methods **2000**, Part. Technol. Series.

[24] J. Israelachvili, *Intermolecular and Surface Forces, second edition*, Academic Press, London, **1992**.

[25] A. K. Hipp, G. Storti, M. Morbidelli, On multiple-particle effects in the acoustic characterization of colloidal dispersions, *Journal of Physics D: Applied Physics* **1999**, 32, 568-576.

[26] D. J. Mc Clements, M. J. W. Povey, Scattering of ultrasounds by emulsions, *Journal of Physics D: Applied Physics* **1989**, 22-38.

## Tables

Table 1: Mean diameter calculated for the measured diffuse transmittance over a concentration range and based on the Percus-Yevick model.

Table 2: Diffusion coefficient  $D_0$  ( $\text{m}^2\text{s}^{-1}$ ), hydrodynamic diameter  $d_H$  (nm), Debye length  $1/\kappa$  (nm) and particle diameter  $d$  (nm) for Klebosol 30R50 suspension and a Klebosol 30R50 suspension in a  $10^{-2}$  M KCl solution.

Table 3: Physicochemical properties of the silica-water system (Units used by the software).

## Legends of illustrations

Fig. 1: Interaction energy diagram of 80 nm particles of Klebosol 30R50.

Fig. 2: Experimental and theoretical transmitted fluxes versus Klebosol 30R50 concentration.

Fig. 3a: Transmission level of the initial silica suspension (15.3% v/v) along the cell height.

Fig. 3b: Transmission level of the diluted silica suspension (1.3% v/v) along the cell height.

Fig. 4: Number and volume PSD determined by laser diffraction for Klebosol 30R50 15.3% v/v.

Fig. 5: Theoretical profiles of diffuse transmittance versus particle diameter for different solid concentrations determined by the Percus-Yevick model.

Fig. 6: Mean diameter measured by PCS versus solid concentration for two suspensions of different salinities: Klebosol 30R50 and Klebosol 30R50 + KCL  $10^{-2}$  M.

Fig. 7: PSD determined by PCS for Klebosol 30R50 at different concentrations.

Fig. 8: Attenuation excess spectra of Klebosol 30R50 for different concentrations.

Fig. 9: Normalized attenuation spectra of Klebosol 30R50 for different concentrations.

Fig. 10: Sound Attenuation through Klebosol 30R50 versus solid concentration for different frequencies.

Fig. 11: Interparticle distance depending on the concentration and viscous and thermal skin depth versus frequency.

Fig. 12: PSD determined by acoustic spectroscopy for Klebosol 30R50 at different concentrations: Concentration imposed.

Fig. 13: PSD determined by acoustic spectroscopy for Klebosol 30R50 at different concentrations: Mean diameter imposed.

Fig. 14: Comparison between the experimental attenuation spectrum of 2.22% and 4.51% v/v of Klebosol 30R50 and the modelling attenuation spectra obtained with the parameters (geometric mean and geometric standard deviation) of the distribution gave by laser diffraction for various concentrations.

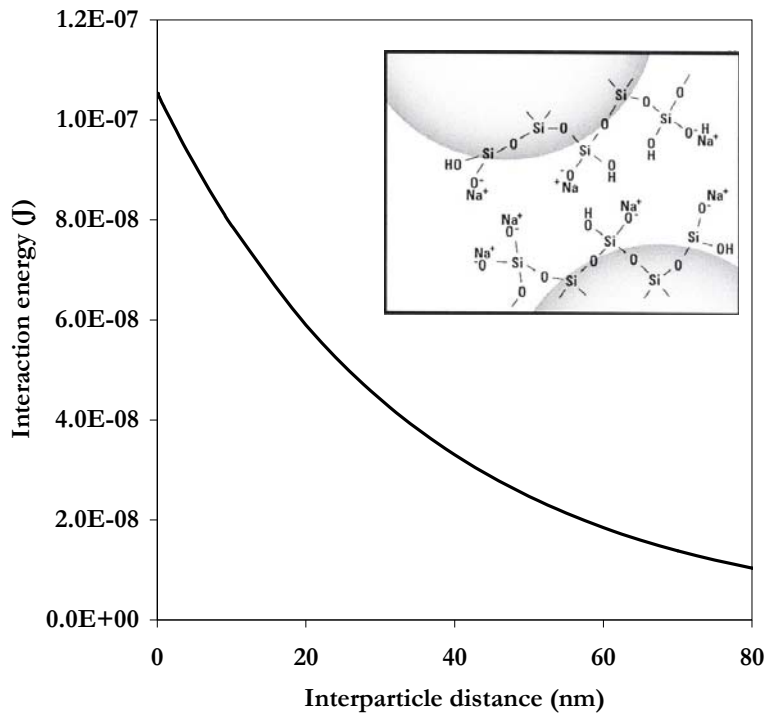


Fig. 1. Interaction energy diagram of 80 nm particles of Klebosol 30R50.

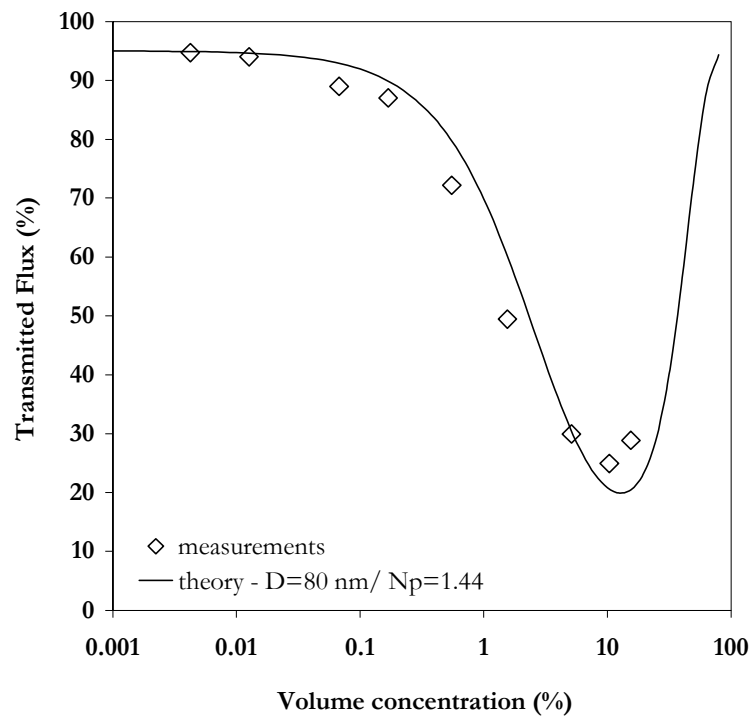


Fig. 2. Experimental and theoretical transmitted fluxes versus Klebosol 30R50 concentration.

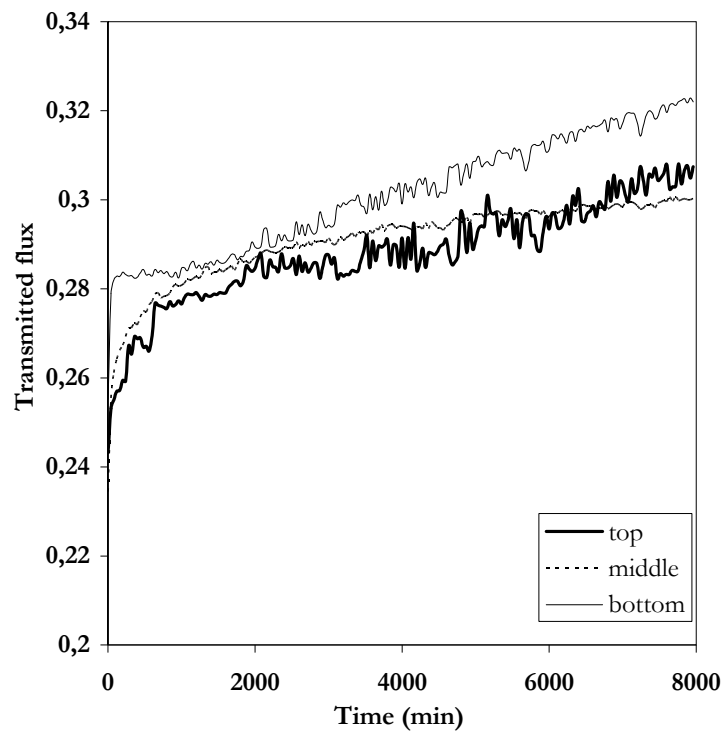


Fig. 3a. Transmission level of the initial silica suspension (15.3% v/v) along the cell height.

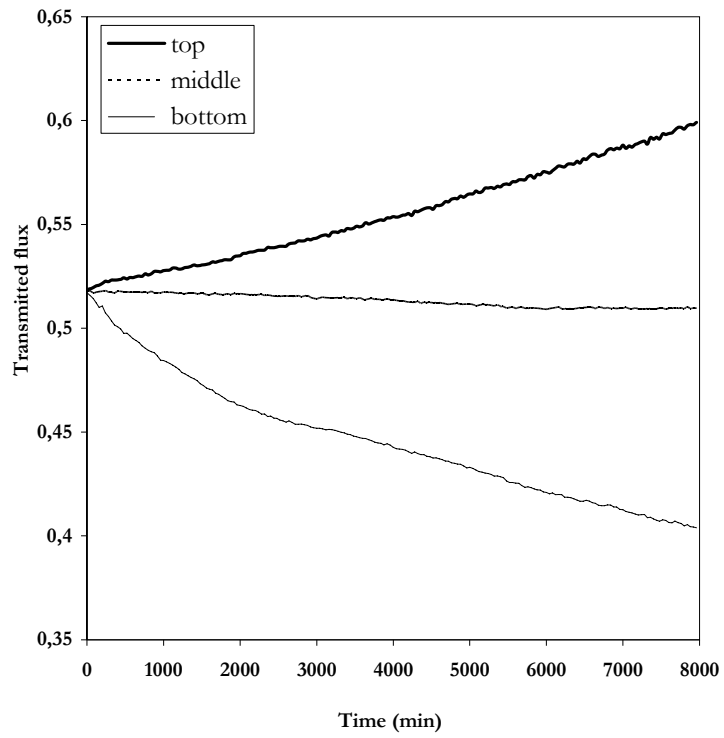


Fig. 3b. Transmission level of the diluted silica suspension (1.3% v/v) along the cell height.

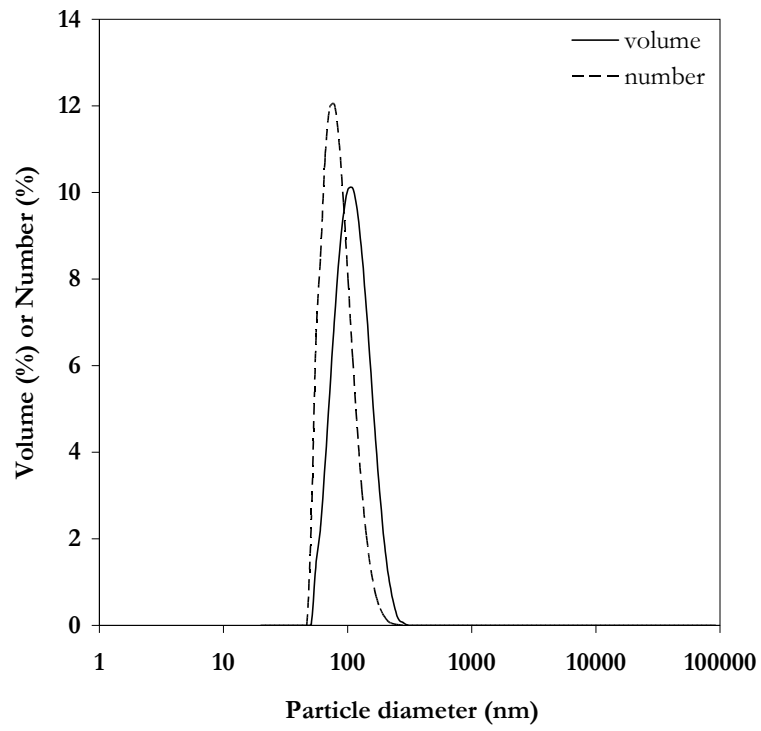


Fig. 4. Number and volume PSD determined by laser diffraction for Klebosol 30R50 15.3% v/v.

Volume concentration (%)	15.3 %	9.62 %	4.51 %	2.63 %	1.30 %
Transmitted flux (%)	14.4	18.1	24.1	35.8	49.7
Calculated $d_{32}$	87 nm	84 nm	89 nm	91 nm	98 nm

Table 1: Mean diameter calculated for the measured diffuse transmittance over a concentration range and based on the Percus-Yevick model.

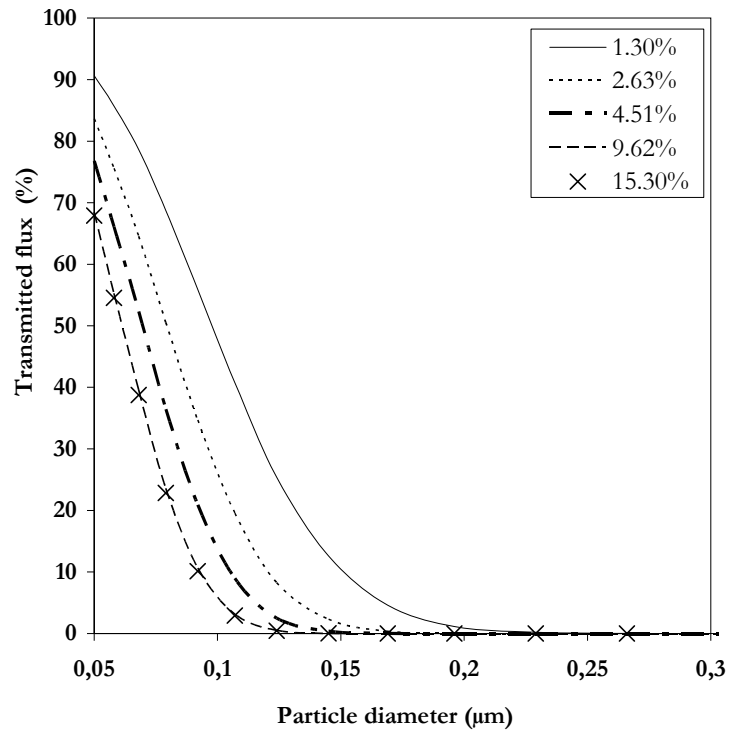


Fig. 5. Theoretical profiles of diffuse transmittance versus particle diameter for different solid concentrations determined by the Percus-Yevick model.

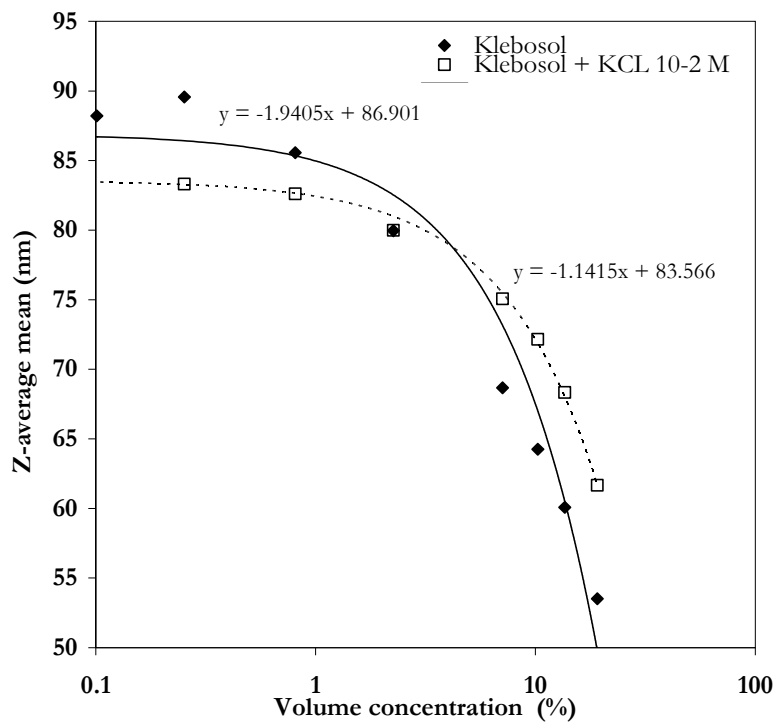


Fig. 6. Mean diameter measured by PCS versus solid concentration for two suspensions of different salinities: Klebosol 30R50 and Klebosol 30R50 + KCL 10<sup>-2</sup> M.

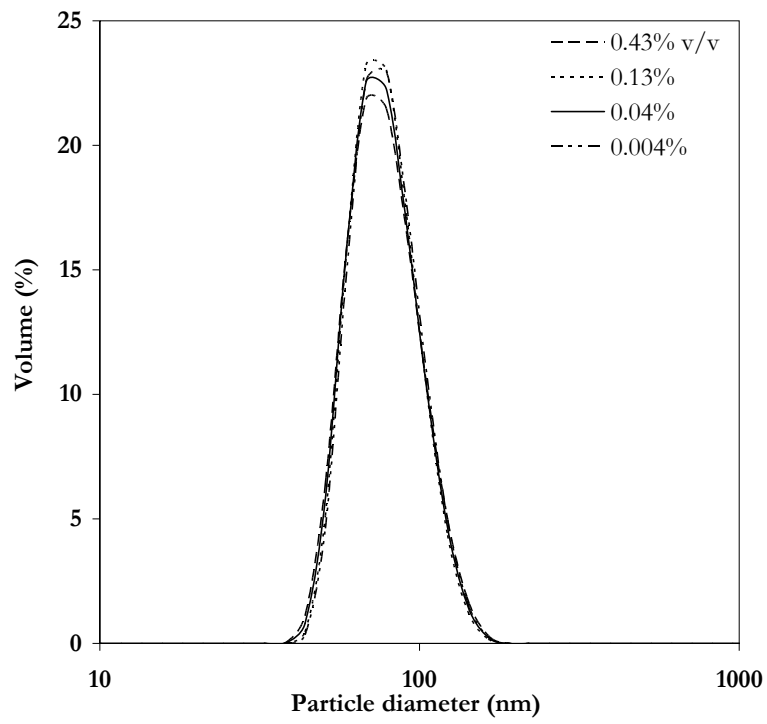


Fig. 7. PSD determined by PCS for Klebsol 30R50 at different concentrations.

suspension	$D_0$ (m <sup>2</sup> .s <sup>-1</sup> )	$d_H$ (nm)	$1/\kappa$ (nm)	$d$ (nm)
Klebosol	4.98 10 <sup>-12</sup>	87.7	34.4	53.3
Klebosol + KCl 10 <sup>-2</sup> M	5.19 10 <sup>-12</sup>	80.8	2.1	78.7

Table 2. Diffusion coefficient  $D_0$  (m<sup>2</sup>s<sup>-1</sup>), hydrodynamic diameter  $d_H$  (nm), Debye length  $1/\kappa$  (nm) and particle diameter  $d$  (nm) for Klebosol 30R50 suspension and a Klebosol 30R50 suspension in a 10<sup>-2</sup> M KCl solution.

Physical properties	Silica	Water
Density (g.cm <sup>-3</sup> )	2.3692	9.9524 10 <sup>-1</sup>
Sound speed (cm.s <sup>-1</sup> )	5.9600 10 <sup>3</sup>	1.4970 10 <sup>5</sup>
Thermal dilatation coefficient (°C <sup>-1</sup> )	1.5600 10 <sup>-6</sup>	2.5677 10 <sup>-4</sup>
Thermal conductivity (erg.cm <sup>-1</sup> .s <sup>-1</sup> .° C <sup>-1</sup> )	1.3703 10 <sup>5</sup>	5.9525 10 <sup>4</sup>
Heat capacity (erg.g <sup>-1</sup> .° C <sup>-1</sup> )	7.4200 10 <sup>6</sup>	4.1785 10 <sup>7</sup>
Shear rigidity (dynes.cm <sup>-2</sup> )	3.1300 .10 <sup>11</sup>	
Viscosity (Po)		9.0300 10 <sup>-3</sup>
Attenuation factor (dB.inch <sup>-1</sup> )	3.75 10 <sup>-5</sup>	4.8539 10 <sup>-3</sup>
Attenuation exponent	2.0000	2.0000

Table 3. Physicochemical properties of the silica-water system (units used by the software)

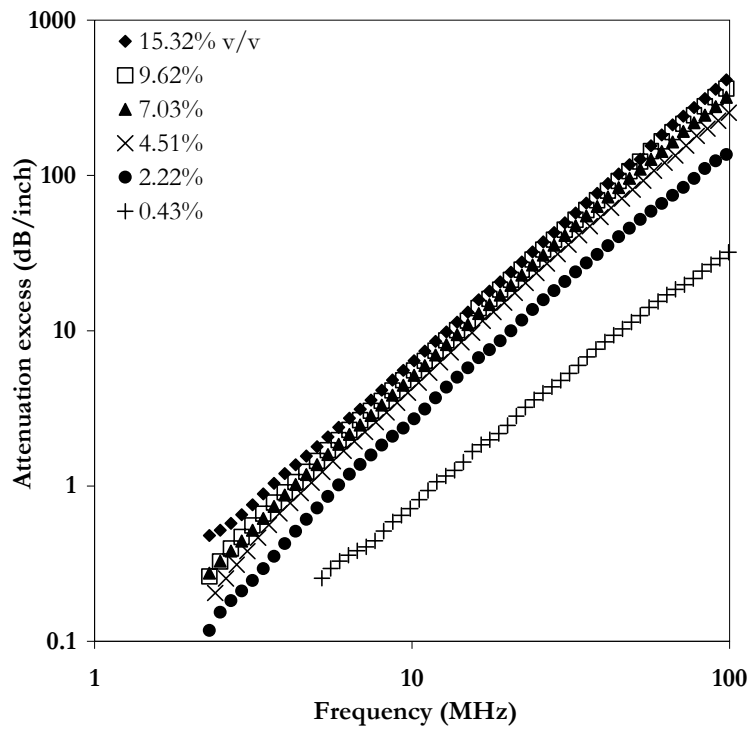


Fig. 8. Attenuation excess spectra of Klebsol 30R50 for different concentrations.

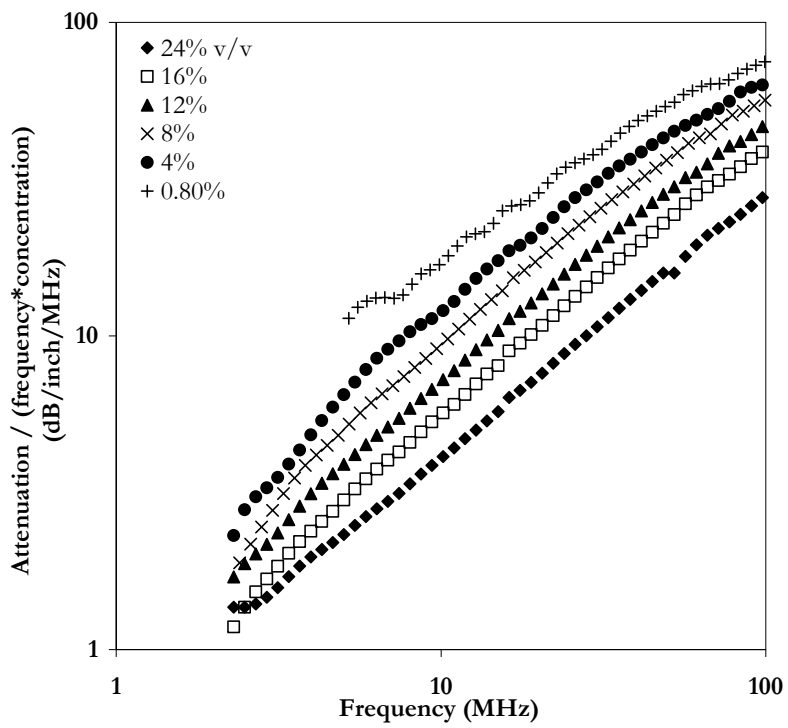


Fig. 9. Normalized attenuation spectra of Klebosol 30R50 for different concentrations.

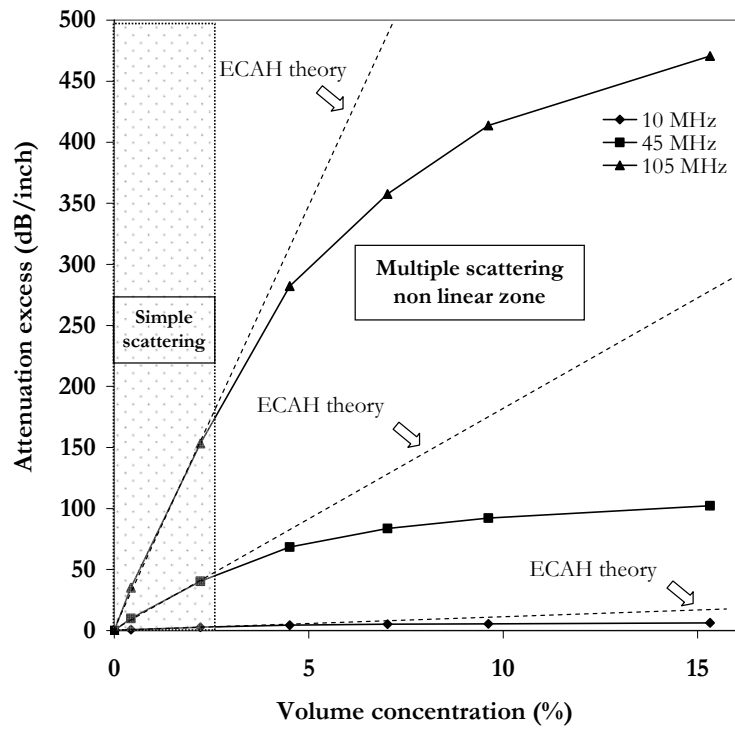


Fig. 10. Sound attenuation through Klebosol 30R50 versus solid concentration for different frequencies.

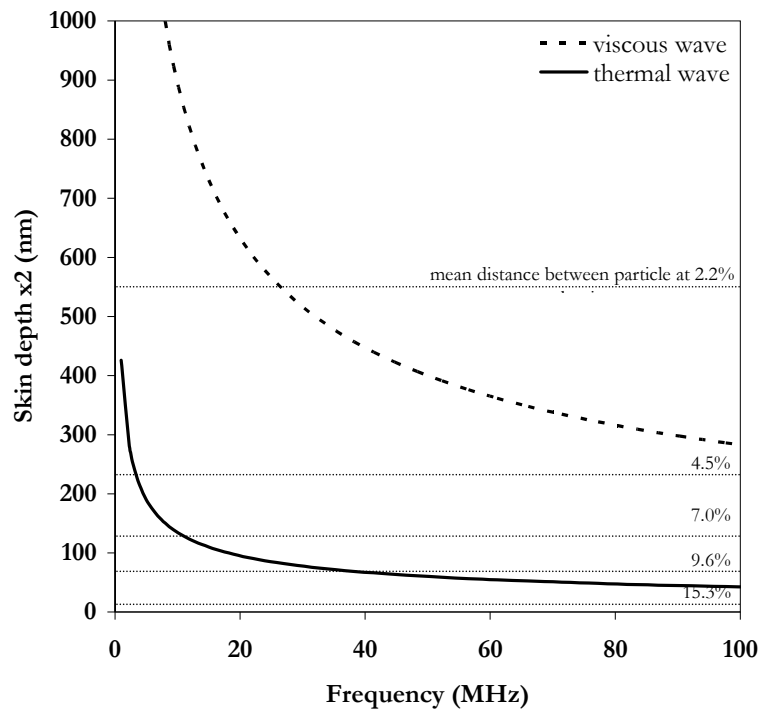


Fig. 11. Interparticle distance depending on the concentration and viscous and thermal skin depth versus frequency.

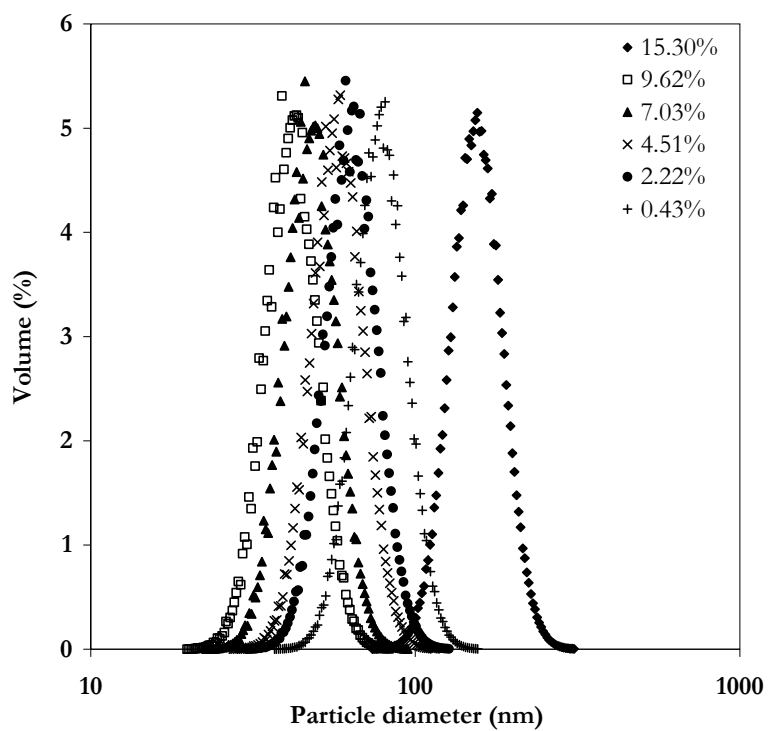


Fig. 12. PSD determined by acoustic spectroscopy for Klebosol 30R50 at different concentrations: Concentration imposed.

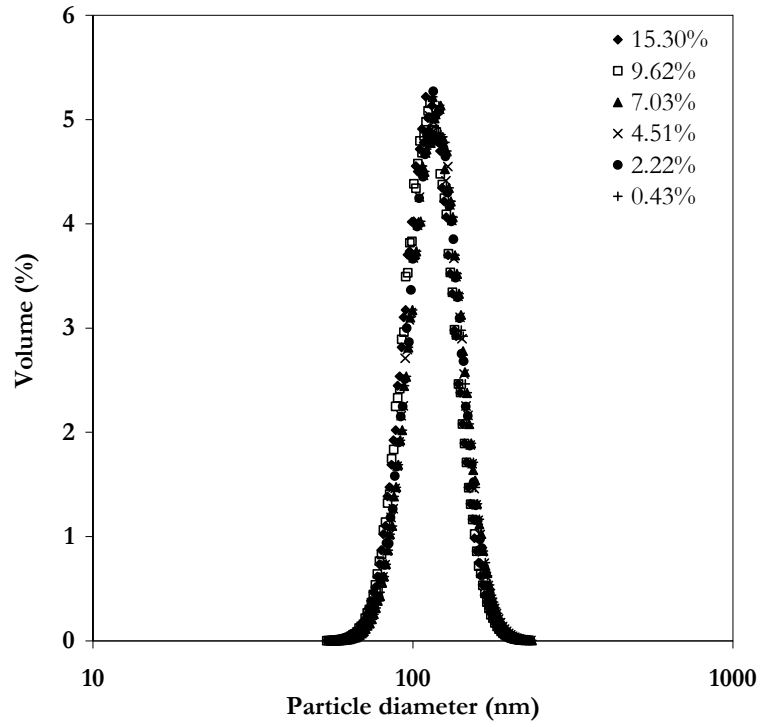


Fig.13. PSD determined by acoustic spectroscopy for Klebosol 30R50 at different concentrations: Mean diameter imposed.

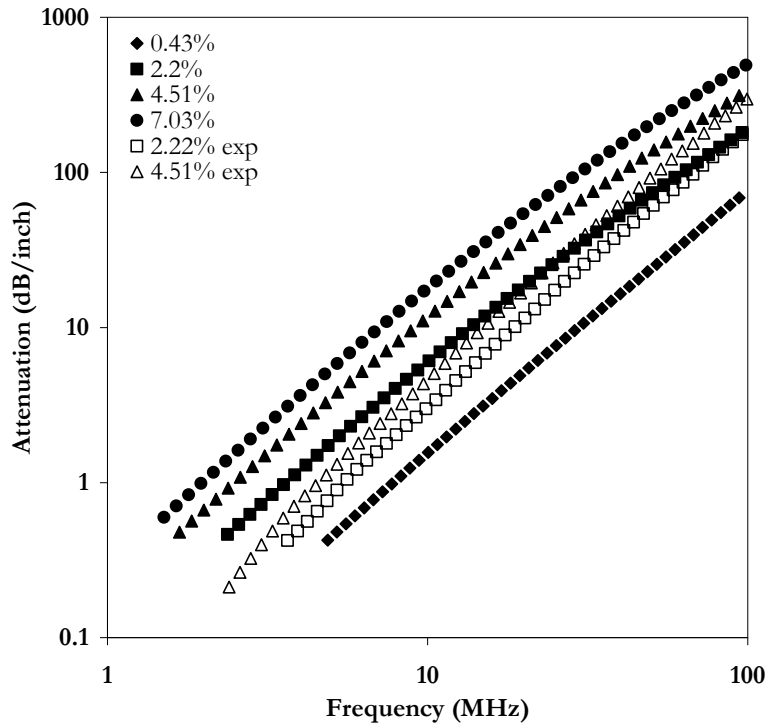


Fig. 14. Comparison between the experimental attenuation spectrum of 2.22% and 4.51% v/v of Klebsol 30R50 and the modelling attenuation spectra obtained with the parameters (geometric mean and geometric standard deviation) of the distribution gave by laser diffraction for various concentrations.